The EMBO Journal (2007) 26, 1953–1962 | © 2007 European Molecular Biology Organization | All Rights Reserved 0261-4189/07
www.embojournal.org

THE EMBO JOURNAL

Structural basis for ARF1-mediated recruitment of ARHGAP21 to Golgi membranes

Julie Ménétrey[1,2,4], Mylène Perderiset[1,2,4], Jérome Cicolari[1,2], Thierry Dubois[1,2,5], Nadia Elkhatib[1,2], Fatima El Khadali[1,2], Michel Franco[3], Philippe Chavrier[1,2] and Anne Houdusse[1,2,*]

[1]Institut Curie, Centre de Recherche, Paris, France, [2]CNRS, UMR144, Paris, France and [3]CNRS, UMR6097, Valbonne, France

ARHGAP21 is a Rho family GTPase-activating protein (RhoGAP) that controls the Arp2/3 complex and F-actin dynamics at the Golgi complex by regulating the activity of the small GTPase Cdc42. ARHGAP21 is recruited to the Golgi by binding to another small GTPase, ARF1. Here, we present the crystal structure of the activated GTP-bound form of ARF1 in a complex with the Arf-binding domain (ArfBD) of ARHGAP21 at 2.1 Å resolution. We show that ArfBD comprises a PH domain adjoining a C-terminal α helix, and that ARF1 interacts with both of these structural motifs through its switch regions and triggers structural rearrangement of the PH domain. We used site-directed mutagenesis to confirm that both the PH domain and the helical motif are essential for the binding of ArfBD to ARF1 and for its recruitment to the Golgi. Our data demonstrate that two well-known small GTPase-binding motifs, the PH domain and the α helical motif, can combine to create a novel mode of binding to Arfs.

The EMBO Journal (2007) **26,** 1953–1962. doi:10.1038/sj.emboj.7601634; Published online 8 March 2007
Subject Categories: structural biology
Keywords: ARF1; ARHGAP21; α-helical motif; PH domain; small GTPases

Introduction

The Ras superfamily of small GTPases regulates a wide variety of cellular processes; these proteins act as molecular switches by cycling between an inactive GDP-bound state and an active GTP-bound state (Takai *et al*, 2001). Guanine nucleotide-exchange factors (GEFs) control their activation by displacing the bound GDP and allowing its replacement with GTP. The active GTP-bound form is inactivated by GTPase-activating proteins (GAPs) that promote hydrolysis of the bound GTP to GDP, thereby returning the protein to its resting state. The conformational changes in small GTPases that are induced by GDP–GTP cycling are located mainly in two regions: the so-called 'switch I' and 'switch II' regions. These conformational changes provide the structural basis for recognition of their effector proteins (Vetter and Wittinghofer, 2001). Among the Ras superfamily, the Arf (ADP-ribosylation factor) proteins are well-characterized regulators of vesicle formation in intracellular traffic (D'Souza-Schorey and Chavrier, 2006), whereas Rho proteins regulate the actin cytoskeleton (Hall, 2005).

The Arf family is distinguished from other small GTPases by a unique structural device, called the 'interswitch toggle', that implements communication between the nucleotide-binding site and a unique N-terminal amphipathic helix that mediates the interaction of Arf proteins with membranes (Antonny *et al*, 1997; Pasqualato *et al*, 2002). In the GDP-bound form of Arf proteins, the amphipathic helix is positioned in a hydrophobic pocket, whereas in the GTP-bound forms it is displaced by the interswitch toggle and stabilizes the interaction of the protein with membrane lipid bilayer. By coupling their GDP–GTP cycle to a cytosol–membrane cycle, Arf proteins are able to regulate vesicular traffic and organelle structure.

The Arf proteins comprise three different subfamilies: the Arfs, Arf-like proteins (Arls), and SARs (Kahn *et al*, 2006). In mammals, the Arf subfamily comprises five members, ARF1–6 (with no ARF2). ARF1 and ARF6 are the most distantly related (67% sequence identity) and they are located at distinct cellular sites, the Golgi complex and the early endosome–plasma membrane interface, respectively. ARF1 is well known for its role in vesicle budding and Golgi regulation through the recruitment of coat proteins and in the regulation of lipid-modifying enzymes and actin-organizing components (for a review see D'Souza-Schorey and Chavrier, 2006). To promote actin assembly, ARF1 facilitates Arp2/3 complex-dependent actin polymerization in a cascade that involves the coat protein COPI, the Rho protein Cdc42 and its downstream effector N-WASP (Stamnes, 2002). Recently, we identified a human GTPase-activating protein for Rho (a RhoGAP), called ARHGAP21 (also referred as ARHGAP10; Dubois *et al*, 2005; Sousa *et al*, 2005), which is recruited by GTP-bound ARF1 to the Golgi complex where it regulates the Arp2/3 complex and F-actin dynamics by controlling Cdc42 activity (Dubois *et al*, 2005). Besides its role in the regulation of actin assembly on Golgi membranes, ARHGAP21 has also been shown to interact with α-catenin, a component of cell–cell junctions in epithelial cells (Sousa *et al*, 2005).

ARHGAP21 is a large protein of 1957 amino-acid residues that contains an N-terminal PDZ domain, a central pleckstrin homology (PH) domain and a C-terminal RhoGAP domain linked by regions of unknown structure. We showed previously that ARHGAP21 interacts specifically with the GTP-bound forms of both ARF1 and ARF6 through a region that comprises the PH domain followed by a 60-residue extension of unknown structure (called hereafter the ARF-binding domain; ArfBD) (Dubois *et al*, 2005). PH domains are best

*Corresponding author. UMR 144, Curie Institut, Centre de Recherche, 26 rue d'Ulm Paris 75248, France. Tel.: +33 1 42 34 63 95; Fax: +33 1 42 34 63 82; E-mail: anne.houdusse@curie.fr
[4]These authors contributed equally to this work
[5]Present address: Département de transfert, Institut Curie, Paris 75248, France

Received: 28 November 2006; accepted: 6 February 2007; published online: 8 March 2007

known for their ability to target cellular membranes by binding specifically to phosphoinositides, but more recently it appeared that this is the property of only a small fraction of known PH domains (Lemmon, 2004). On the other hand, small GTPases such as Arf proteins seem to play a role in defining PH domain localization (Levine and Munro, 2002; Godi *et al*, 2004; Lemmon, 2004). We have shown that the PH domain of ARHGAP21 does not bind phosphoinositides in liposomes, suggesting that it is unable to bind to cellular membranes (Dubois *et al*, 2005). ARHGAP21 thus associates with the Golgi through the interaction of its ArfBD with ARF1 and not by the direct association of its PH domain with membrane lipids (Dubois *et al*, 2005).

Here, we present the crystal structure of the ARF1:ArfBD complex at 2.1 Å resolution. Our structural and biochemical data show that ArfBD forms a tight complex with ARF1 through two juxtaposed binding motifs, a PH domain and a helical motif, which are both critical for complex formation. Structural comparisons reveal that the PH domain of ARHGAP21 undergoes rearrangements upon ARF1 binding and also explain why it does not bind phosphoinositides. Lastly, our structure highlights a hydrophobic triad patch in Arf proteins as a structural determinant for effector binding.

Results

Structure determination

An N-terminally truncated and GTP-locked (Q71L) mouse ARF1 mutant comprising residues 16–180 (hereafter called ARF1) and the Arf-binding domain of ARHGAP21 (ArfBD; residues 929–1096) were each expressed in *Escherichia coli*. The complex was formed by mixing purified ARF1 and ArfBD proteins and isolated from the mixture by gel filtration chromatography. Dynamic light-scattering measurements showed that the ARF1:ArfBD complex has a molar ratio of 1:1 (data not shown). Best crystals grew in the $P2_1$ monoclinic space group and diffracted up to 2.1 Å. We determined the structure by a combination of the molecular replacement method (for ARF1) and manual fitting and building (for ArfBD) in electron density maps calculated using phases from the molecular replacement solution (see the Materials and methods section). The asymmetric unit contains six complexes that are virtually identical with an average root-mean-square deviation (r.m.s.d.) of 0.32 Å calculated for 295 Cα atoms. Three regions of ArfBD are not visible in the electron density map, namely residues 944–955, 979–986 and the 30 C-terminal residues; we assume that they are disordered in the crystal. The current model was refined to working and free *R* factors of 20.0 and 23.5%, respectively. A representative portion of the final electron density map in the region of ArfBD is shown in Supplementary Figure S1. Statistics of structure determination and refinement are summarized in Table I.

Table I Data collection and refinement

Data set[a]	ARF1:ArfBD
Space group	$P2_1$
Cell dimensions	
a, *b*, *c* (Å)	74.6, 132.1, 146.3
β (deg)	90.01
No. of cplx/ua	6
Data collection	
Resolution (Å)	50–2.1 (2.21–2.1)
Observed reflections	615 527
Unique reflections	155 860
Mosaicity	0.6
R_{sym}[b] (%)	8.8 (36.9)
Mean$\langle I/\sigma I\rangle$	14.6 (3.8)
Completeness (%)	98.4 (95.5)
Bwilson (Å^2)	25.0
Refinement	
Resolution (Å)	50–2.1
R_{work}[c]/R_{free}[c] (%)	20.0/23.5
No. of non-H atoms	
Proteins	15 052
Solvent	1656
Mg^{2+} GTP	210
Dioxane	18
Average *B*-factor (Å^2)	23.0
R.m.s.d.	
Bond length (Å)	0.007
Bond angles (deg)	1.113

[a]Values in parantheses are for the highest resolution shells.
[b]$R_{sym} = \sum_{hkl}\sum_i|I_i - \langle I\rangle|\sum_{hkl}\sum_i I_i$.
[c]$R_{work} = \sum_{hkl}||F_{obs}| - k|F_{calc}||/\sum_{hkl}|F_{obs}|$, R_{free} was calculated using 10% of data excluded from refinement.

ARF1:ArfBD structure

In the ARF1:ArfBD structure, ARF1 contains the G domain fold typical of the Ras superfamily with a central six-stranded β sheet (β1–β6 strands) flanked by five α helices (α1–α5 helices) (Figure 1A). The overall fold, the switch conformations and the Mg.GTP-binding site of ARF1 in the complex are very similar to those of $ARF1_{GTP}$ alone (r.m.s.d. of 0.51 Å on 162 Cα atoms; PDB code 1O3Y; Shiba *et al*, 2003). Its binding partner ArfBD is folded into a PH domain (residues 939–1038) connected to a long C-terminal α helix (αCter helix; residues 1042–1063) by a three-residue linker (Figure 1A). The core of the PH domain is an antiparallel β sheet consisting of seven strands (β1′–β7′ strands) with a C-terminal α helix (α1′ helix) (Figure 1A). The αCter helix makes van der Waals contacts with the tip of the β5′–β6′–β7′ sheet of the PH domain sustained with (i) bipartite hydrogen bonds between Arg1055 and the carbonyl main chains of the β6′-β7′ loop (T1012–S1013) and (ii) a hydrophobic clamp between Leu1052 of the αCter helix and Leu994 of the PH domain (Figure 1B). Also, Leu1041 from the three-residue linker inserts between the PH domain and the αCter helix contributing to additional hydrophobic interactions (Figure 1B). The interface between the PH domain and the αCter helix of ArfBD buries an average of 989 Å^2 surface area.

The ARF1:ArfBD interface can be described as two adjacent contact areas that involve the PH domain and the αCter helix of ArfBD (Figure 1A). Both contact areas cover surfaces of similar size with the total interface area burying an average of 1652 Å^2. The PH domain of ArfBD makes two sets of interactions with the interswitch and switch I regions of ARF1. First, the β5′ strand and the following β5′–β6′ loop (called hereafter the β5′ region) of ArfBD fit into a groove of ARF1 lined by a six-residue stretch (43-VTTIPT-48) of switch I on one side, the interswitch (N52) on the other side and residues of the α1 helix at the bottom (Figure 1C). Tyr999, which belongs to the β5′ region, is a central residue of this contact area (Figure 1A). It plugs into the groove making hydrophobic contacts with Thr31, Tyr35 and Leu39 of the

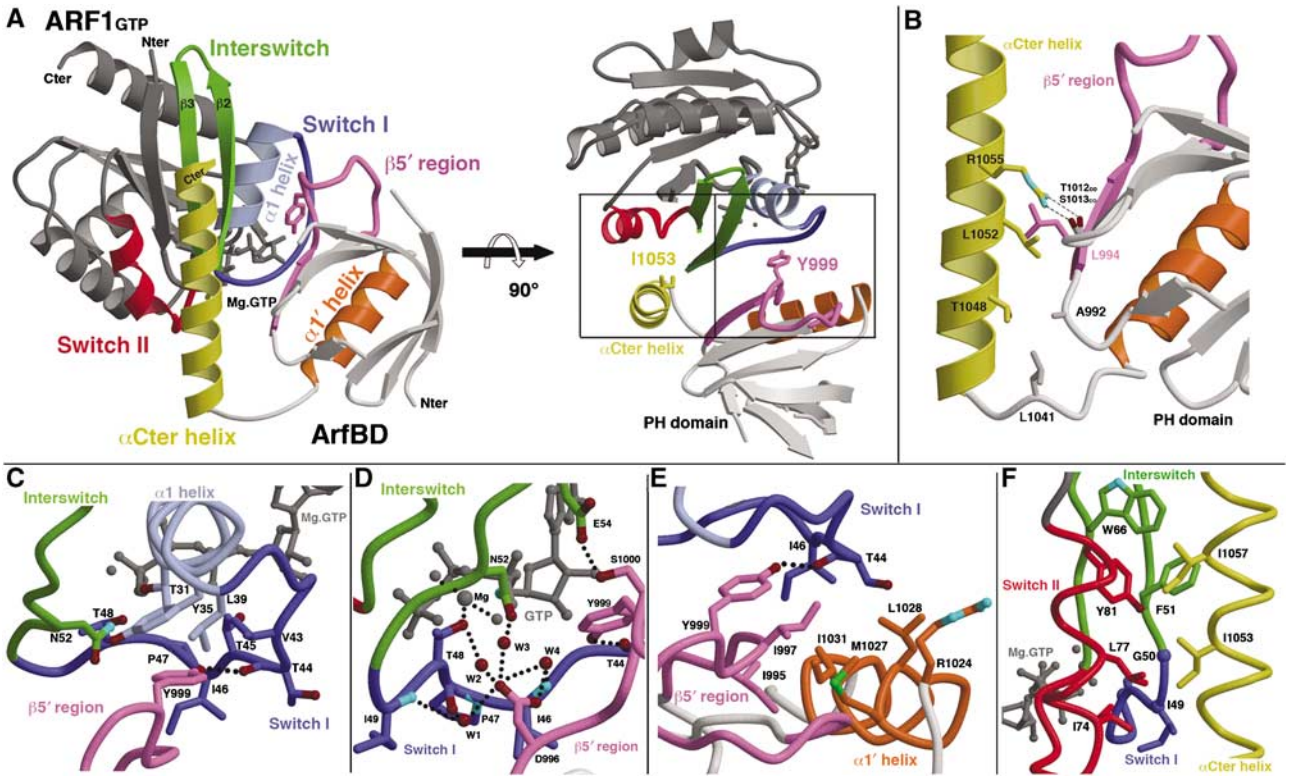

Figure 1 Structure of the ARF1:ArfBD complex. (**A**) A cartoon diagram of the ARF1:ArfBD complex is shown in two distinct orientations. ARF1 is shown in grey with the α1 helix and switch I region in light and dark blue, respectively, the interswitch region in green and the switch II region in red. The Mg.GTP ligand is shown as a grey stick model. ArfBD is shown in white with its β5′ region (β5′ strand plus β5′–β6′ loop) in pink, the α1′ helix in orange and the αCter helix in yellow. Tyr999 and Ile1053 of ArfBD are shown as stick models. The two adjacent contact areas of the ARF1:ArfBD complex interface are delineated by black boxes on the right-hand view. (**B**) Detailed view of the interface between the αCter helix and the PH domain of ArfBD. (**C–F**) Detailed views of the ARF1:ArfBD interface. The secondary structures are shown as ribbons and the residues as sticks. Hydrogen bonds are indicated by dashed lines. (C) The β5′ region of ArfBD (pink) lies between the interswitch (green) and switch I (blue) regions of ARF1 centred on Tyr999. (D) The network of water-mediated interactions made between Asp996 of the β5′ region (in pink) of ArfBD and ARF1. (E) The switch I (blue) region of ARF1 interacts with the β5′ region (pink) and the α1′ helix (orange) of ArfBD. (F) The αCter helix (yellow) of ArfBD is grasped between the switch II (red) and the interswitch/switch I (green/blue) regions of ARF1.

α1 helix, and Val43 and Thr45 of switch I. Also, Tyr999 side-chain hydroxyl makes a direct hydrogen bond with the main-chain carbonyl of Thr44 and a water-mediated interaction with the main-chain amide of Ile46. Another residue of the β5′ region, Asp996, also plugs inside this groove of ARF1 making a network of water-mediated hydrogen bonds with residues 46-IPTI-49 of switch I and Phe51-Asn52 of the interswitch (Figure 1D). Among these water-mediated interactions is the hydroxyl group of Thr48 that directly contacts both the magnesium ion and the gamma phosphate of the Mg^{2+}.GTP ligand (Figure 1D). The second set of interactions involves the switch I region of ARF1 that inserts Thr44 and Ile46 into a groove of ArfBD making extensive hydrophobic interactions with Ile995, Ile997 and Tyr999 of the β5′ region on one side and Arg1024 (aliphatic side chain), Met1027, Leu1028 and Ile1031 of the α1′ helix on the other side (Figure 1E).

The αCter helix of ArfBD, involved in the second contact area, is grasped between switch I and switch II of ARF1 aligned along the interswitch β2−β3 strands (Figure 1F). This contact area, which is mainly hydrophobic, is centered around residue Ile1053 of ArfBD that interacts with both switch I and switch II (Figure 1A and F). Ile1053 faces a hydrophobic pocket of ARF1 interacting with residues Ile49-Gly50 of switch I and Phe51 of the interswitch (β2 strand) on one side, and with residues Ile74, Leu77 and Tyr81 of switch II (α2 helix) on the other side (Figures 1F and 2). Note that these interactions are possible because Gly50 undergoes torsional changes that trigger the carbonyl group of Ile49 to flip outside the hydrophobic pocket where it resides normally in the unbound $ARF1_{GTP}$ structure (Goldberg, 1998; Shiba *et al*, 2003). Another residue of the αCter helix, Ile1057, also contributes to this hydrophobic contact area interacting with a hydrophobic triad patch in ARF1 composed of Phe51, Trp66 and Tyr81 of the interswitch and switch II, respectively (Figures 1F and 2A).

ARHGAP21 specificity

This structure provides a rationale for the specificity of ArfBD for the GTP-bound form of ARF1, as most of the interface residues belong to the switch I, switch II and interswitch regions of ARF1, which drastically differ in conformation in the GDP-bound form (Supplementary Figure S2). Also, our structure explains why ArfBD can also bind ARF6 as reported in *in vitro* studies (Dubois *et al*, 2005). All the interface residues involved in ARHGAP21 binding are indeed virtually identical in ARF1 and ARF6, except for one conserved sequence difference lining the hydrophobic pocket (I49 versus V46, respectively; Figure 2B). In contrast, in Arl and SAR subfamilies, interface residues are less conserved (Figure 2B), suggesting that ARHGAP21 probably does not bind to them.

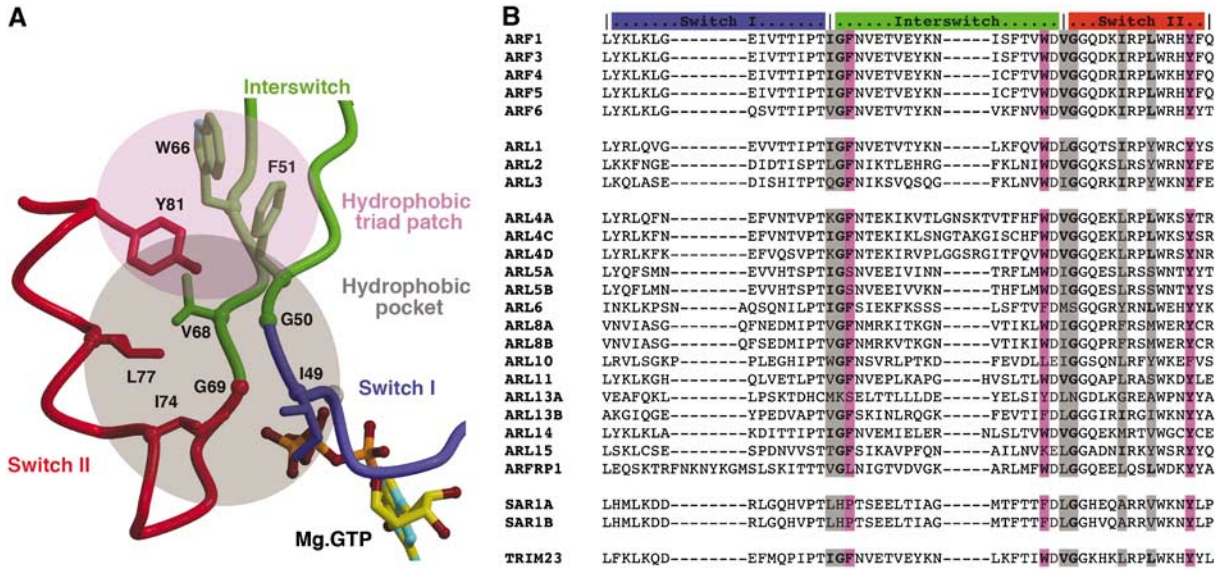

Figure 2 The hydrophobic pocket and triad patch of Arf proteins. (**A**) Front-view of the ARF1 hydrophobic pocket (transparent grey area) and the hydrophobic triad patch (transparent purple area) with the hydrophobic residue side chains shown as stick models. (**B**) Sequence alignment of the Arf proteins (nomenclature from Kahn *et al*, 2006) with residues of the hydrophobic pocket indicated with grey shading and those of the triad patch indicated in purple. Residues conserved with ARF1 are shown in bold.

Altogether, our data reveal that ARHGAP21 is an effector for the Arf subfamily proteins (Dubois *et al*, 2005; this study).

Structural rearrangements of ARHGAP21-PH domain upon ARF1 binding

The NMR structure of the unbound PH domain of ARHGAP21 has been solved recently by the RIKEN Structural Genomics/Proteomics Initiative (RSGI; PDB code 2DHJ; Li *et al*). The overall fold of the unbound PH domain is similar to that of ArfBD bound to ARF1 (r.m.s.d. in the range of 0.71–1.04 Å and an average of 0.87 Å on 80 Cα atoms) (Figure 3A). One striking difference is the β5′–β6′ loop that diverges dramatically when compared to the ARF1-bound form. The Tyr999 side chain flips towards ARF1 and the Ser1000-Glu1001 main-chain polypeptide undergoes large rearrangements between these two forms (largest Cα displacements observed for residues S1000 and E1001 are 5.5 and 7.6 Å, respectively) (Figure 3B). Note that we exclude that these structural rearrangements could be the consequence of the αCter helix interaction with the PH domain in ArfBD (absent in the unbound PH domain structure), as no significant structural difference is found at the interface and the β5′–β6′ loop is not directly in contact with the αCter helix. Superposition of the PH domain of the unbound form to that of the ARF1:ArfBD complex reveals that steric hindrance will occur between the Leu39 side chain of ARF1 and the β5′–β6′ loop of the PH domain (Ser1000 main chain; Figure 3B). This suggests that ARF1 binding triggers the β5′–β6′ loop conformational change of the PH domain of ArfBD and induces Tyr999 flipping towards the switch I of ARF1. This further highlights the central role of Tyr999 in ARF1:ArfBD interaction.

Cellular localization and affinity measurements

As previously reported (Dubois *et al*, 2005), GFP-tagged ArfBD localized to the Golgi complex when overexpressed in HeLa cells, as seen by its colocalization with the medial-Golgi protein GM130 by immunofluorescence microscopy (Figure 4A–C, arrows), whereas the PH domain alone (deletion of the C-terminal extension of ArfBD) no longer localized to the Golgi complex and rather accumulated in the cytosol (Figure 4D–F). Analytical ultracentrifugation affinity measurements revealed that the affinity of the PH domain alone for Δ17-ARF1$_{GTP}$-Q71L is reduced by 650-fold when compared to the ArfBD ($K_d = 55$ nM; see Supplementary Table SI). These observations show that the PH domain alone is not sufficient for recruitment to Golgi membranes and to bind ARF1; the C-terminal extension is required. This supports the notion that the localization of ArfBD on the Golgi depends on its interaction with GTP-bound ARF1.

To examine the roles of residues Tyr999 of the PH domain and Ile1053 of the αCter helix of ArfBD in the formation of the complex, we created variants of ArfBD by using site-directed mutagenesis and tested their cellular localization and interaction with GTP-bound ARF1 *in vitro*. Substitution of Tyr999 or Ile1053 with alanine resulted in accumulation of the mutated protein in the cytosol when overexpressed in HeLa cells (Figure 4). Of note, the effect of these mutations in the context of the intact protein could not be analysed, as we were unable to obtain expression of full-length ARHGAP21 upon transfection of HeLa cells (Dubois *et al*, 2005). Analytical ultracentrifugation affinity measurements revealed that Y999A and I1053A mutations reduced the affinity of ArfBD for Δ17-ARF1$_{GTP}$-Q71L by 150- and 100-fold, respectively, when compared to the wild-type protein (Supplementary Table SI). These results confirm that Tyr999 and Ile1053 are critical residues of ArfBD for ARF1 interaction. Altogether, these data show that both the PH domain and the αCter helix of ArfBD are essential for complex formation with ARF1.

The activity of the RhoGAP domain of ARHGAP21 is not affected by ARF1 binding

To evaluate whether the interaction of ARF1 with the ArfBD can also affect the stimulation of GTP hydrolysis

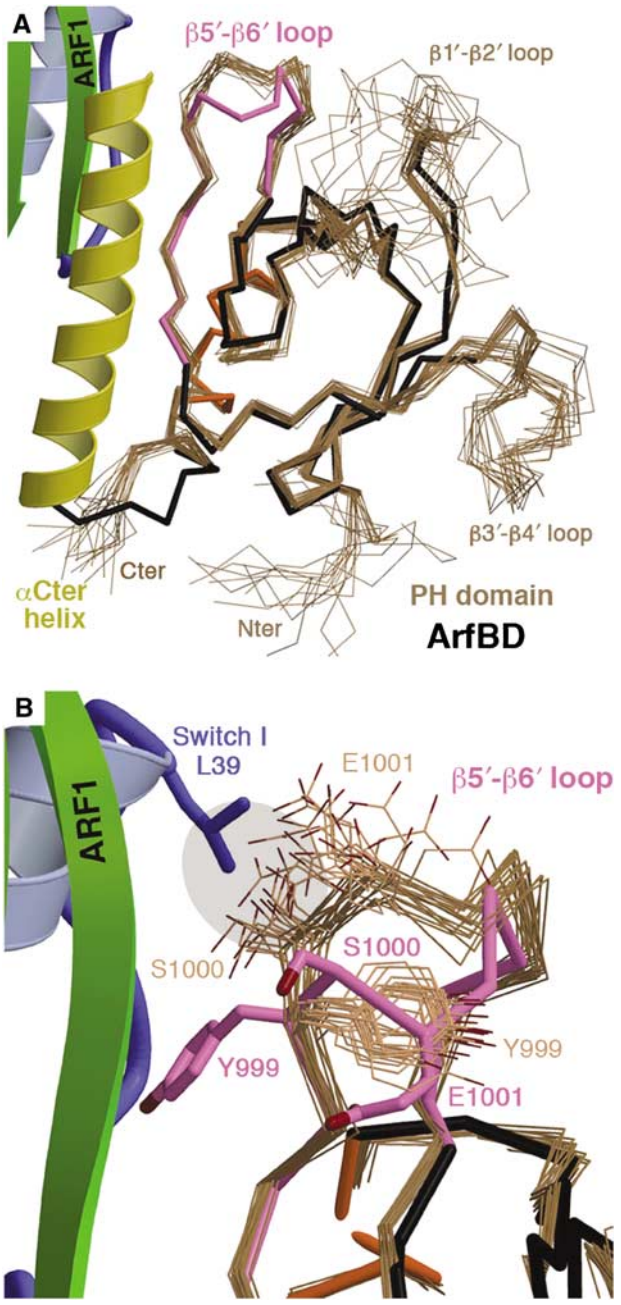

Figure 3 Structural rearrangement of the β5′–β6′ loop of the PH domain upon ARF1 binding. (**A**) Overall superposition of the PH domain of ARHGAP21 of the unbound form on the ARF1-bound form. ARF1 and the αCter helix of ArfBD are shown as a cartoon diagram with the same colour code as in Figure 1. The PH domain of the ARF1-bound form is shown in a black bold trace with the β5′ region and the α1′ helix in pink and orange, respectively. The PH domain of the unbound form (2DHJ; NMR structure with 20 conformers) is shown in thin brown trace. (**B**) Detailed view of the β5′–β6′ loop of the PH domain in the unbound and ARF1-bound form. Residues Tyr999, Ser1000 and Glu1001 are shown for both forms. Leu39 of ARF1 is shown in sticks and area of the steric hindrance between Leu39 and the β5′–β6′ loop is indicated with a grey area.

by the RhoGAP domain of ARHGAP21, GAP activity of a larger construct comprising the ArfBD/RhoGAP domains of ARHGAP21 on Cdc42 was analysed in the presence or absence of activated ARF1. When assayed with proteins in solution, we found no effect of GTP-ARF1 on the GAP activity of ArfBD/RhoGAP towards Cdc42 (Supplementary Figure S3). However, we cannot exclude some effect of ARF1 binding on the GAP activity of full-length ARHGAP21 when all the proteins are bound to membrane (see Discussion).

Structural basis for the inability of ARHGAP21-PH domain to bind phosphoinositides

The observation that the PH domain of ARHGAP21 does not associate with intracellular membranes (Figure 4) together with our previous finding that the PH domain of ARHGAP21 does not bind phosphoinositides in liposomes (Dubois *et al*, 2005) argues that this PH domain is unable to bind lipids. Overall, PH domains bind phosphoinositides in a positively charged groove formed at the β1′–β2′ sheet extremity (Figure 5A), which is composed of amino acids with basic side chains that hydrogen-bond directly with the phosphoinositide phosphates (Lemmon, 2004). In ARHGAP21, this groove is comprised of residues Phe939, Lys958 and Met960 (Figure 5B). Because Phe939 and Met960 do not have basic side chains, this confirms that the PH domain of ARHGAP21 does not bind phosphoinositides (Dubois *et al*, 2005).

A similarity search using the DALI server (http://www.ebi.ac.uk/dali/) revealed that the closest structural relative of the ARHGAP21 PH domain is that of the cytoskeletal protein β-spectrin, which binds phosphoinositides in an unconventional groove between the β1′–β2′ and β5′–β6′ loops (Hyvonen *et al*, 1995) (Figure 5A). Our observation that the β5′–β6′ loop rearranges dramatically upon ARF1 binding (Figure 3B) raises the question of whether ARF1 binding influences the capacity of ARHGAP21 PH domain to interact with phospholipids. Note that two other PH domain-containing proteins, FAPPs and OSBPs, require both ARF1 and phospholipid binding for membrane recruitment (Levine and Munro, 2002; Godi *et al*, 2004). Previously, we have observed that ArfBD was no more recruited to liposomes when incubated with GTP-ARF1 in a form that is unable to interact with membrane (Δ17-ARF1) (Dubois *et al*, 2005). Indeed, Tyr999 is very far from the IP3 location (based on β-spectrin structure) to impact on phospholipid binding (Figure 5B). Finally, structure-based sequence comparisons of the β-spectrin and ARHGAP21 PH domains revealed several differences within this phospholipid-binding site (Figure 5A). Residues Ser22 (β1′–β2′ loop) and Tyr69 (β5′–β6′ loop) of the β-spectrin PH domain make hydrogen bonds with the inositol trisphosphate (IP3) groups; the equivalent positions in ARHGAP21 are occupied by proline and threonine residues (P956 and T1002, respectively), which are unable to make equivalent interactions (Figure 5A and B). Also, residue Glu10 (β1′ strand) in β-spectrin, which directs Lys8 (β1′ strand) to interact with the phosphate group of IP3, is a leucine residue (L942) in ARHGAP21, which probably does not position Arg940 in a similar manner (the equivalent residue to Lys8 in β-spectrin) (Figure 5A and B). Taken together, these differences in sequence in both known phosphoinositide-binding grooves probably account for the inability of the PH domain of ARHGAP21 to bind phosphoinositides.

A shared Arf:effector mode of binding

Of the five Arf:effector complex structures known to date (Supplementary Figure S4), two share a similar mode of binding to that of the ARF1:ArfBD complex, namely

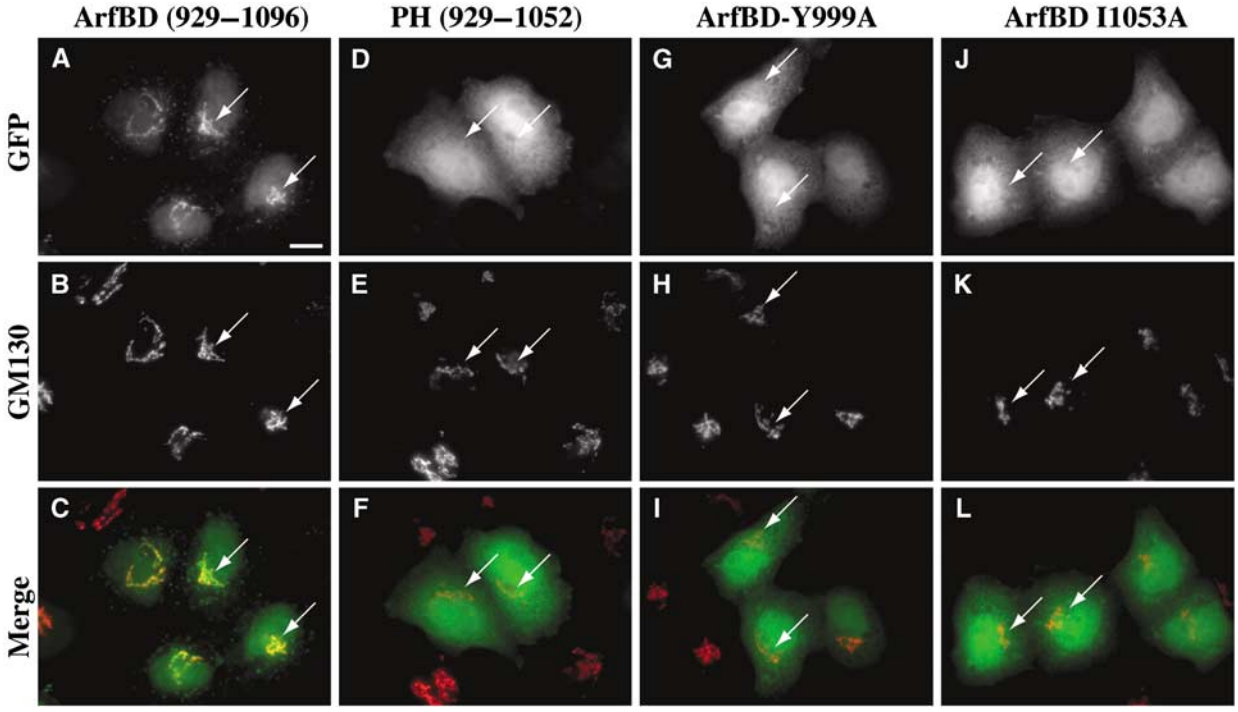

Figure 4 Localization of ArfBD to the Golgi requires both the PH domain and the αCter helix. HeLa cells were transiently transfected with constructs encoding GFP-tagged intact ArfBD (residues 929–1096) (**A–C**), PH domain alone (residues 929–1052) (**D–F**) or ArfBD with a point mutation at Tyr999 in the PH domain (ArfBD-Y999A) (**G–I)** or at Ile1053 in the αCter helix (ArfBD-I1053A) (**J–L)**. Cells were fixed after 16 h and stained with antibodies against GM130, a medial Golgi marker. Upper panels, the GFP signal of the overexpressed constructs. Middle panels, GM130 staining. Lower panels, merged images of the GFP (green) and GM130 (red) signals. Only intact ArfBD colocalizes with GM130 (see arrows pointing to co-localization of ArfBD and GM130 in the Golgi complex). ArfBD-Y999A, ArfBD-I1053A or PH domain alone have a diffuse distribution in the cytosol. Bar, 10 μm.

the NGAT domain of GGA (Shiba *et al*, 2003) and the GRIP domain of Golgin245 (Panic *et al*, 2003; Wu *et al*, 2004) in complex with ARF1 and ARL1, respectively. All three effector domains contain a helical motif that binds Arf proteins by interacting with the switch regions aligned along the inter-switch β-sheet. The helical motif of ArfBD consists of one helix (αCter helix), whereas those of NGAT and GRIP domains are hairpin helix–loop–helix motifs. Superposition of the three complexes shows that the position of the αCter helix of ArfBD is similar to that of the α1 helices of NGAT and GRIP domains, but it is displaced by 4 Å towards the hydrophobic pocket (Figure 6). Thus, whereas the α1 helices of NGAT and GRIP domains contact switch I and the α0/α2 helices contact switch II, the αCter helix of ArfBD contacts both switch I and switch II. (Note that the α3 helix of the GRIP domain does not participate in the binding interface.) The helical motifs of the NGAT and GRIP domains are sufficient to bind their respective Arf partners (Panic *et al*, 2003; Shiba *et al*, 2003; Wu *et al*, 2004), but the αCter helix of ArfBD is clearly insufficient to bind ARF1 even though it contacts both switch I and switch II.

Discussion

ARHGAP21 possesses a PH domain that is necessary but not sufficient for binding to ARF1. An adjacent C-terminal region is required and the interaction of this whole region with ARF1 is also essential for the recruitment of ARHGAP21 to intracellular membranes (Dubois *et al*, 2005). The structure we report here shows that the C-terminal region forms an α helix, the αCter helix, that packs against the PH domain, and both interact with GTP-ARF1. Our binding studies confirm that both the PH domain and the αCter helix (ArfBD) of ARHGAP21 are required for binding to ARF1. Separately, PH domains and helical motifs are well-characterized small GTPase-binding motifs (Lemmon, 2004; Kawasaki *et al*, 2005); however, our study demonstrates that new binding properties can result from the juxtaposition of two distinct binding motifs. In addition to ARHGAP21, two other effectors, GGA and Golgin245, bind Arf proteins through a helical motif (Panic *et al*, 2003; Shiba *et al*, 2003; Wu *et al*, 2004). The Arf-binding domains of GGA and Golgin245, which both fold into a helix–loop–helix structure, are sufficient for binding to their Arf partner (Panic *et al*, 2003; Shiba *et al*, 2003; Wu *et al*, 2004). On the countrary, the ARHGAP21 helical motif consisting of a single helix is insufficient for binding to ARF1. This mode of binding through a helical motif has also been observed for effectors of the Rab family GTPases (Kawasaki *et al*, 2005). Most of these effectors bind Rab proteins through a two-helix motif, but Rabphilin-3A binds Rab3A by means of a single helix and an adjoining SGAWFF structural element, both of which are critical for high-affinity binding (Ostermeier and Brunger, 1999). Similarly, an extended region N-terminal to the PH-like domain of RanBP2-RanBD1 interacts with the GTPase Ran and is critical for its binding affinity (Vetter *et al*, 1999; Villa Braslavsky *et al*, 2000). Thus, ARHGAP21, Rabphilin-3A and RanBP2 bind to their respective GTPase partners through a combination of two motifs, both of which are crucial for the interaction. This illustrates the potential importance of adjacent regions or domains

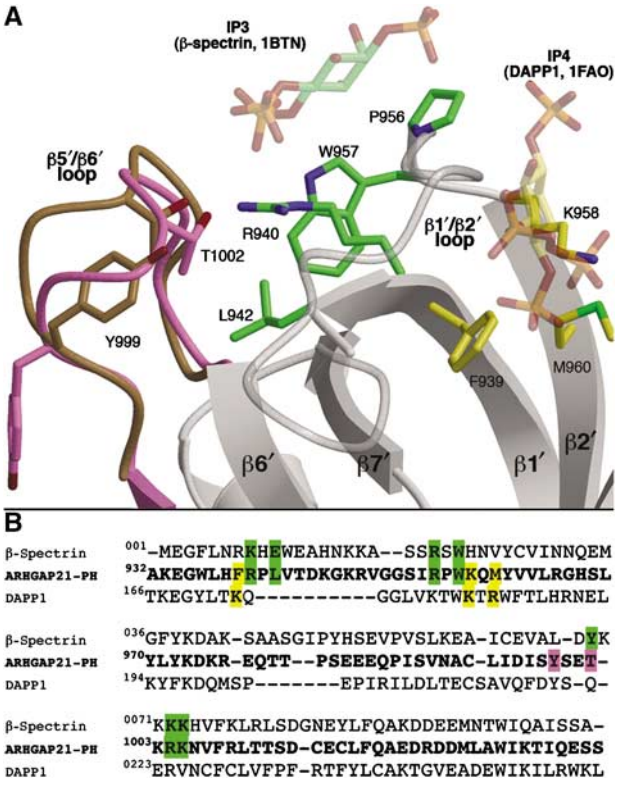

Figure 5 Phosphoinositide-binding sites in the PH domain of ARHGAP21. (**A**) A detailed view of both putative 'phosphoinositide-binding' sites in the PH domain of ARHGAP21. Residues of ARHGAP21 equivalent to those involved in the phosphoinositide-binding site in β-spectrin and DAPP1 are shown in pink and yellow, respectively. The position of IP3 and IP4 ligands in the β-spectrin PH domain (1BTN) and DAPP1 PH domain (1FAO) structures, respectively, are shown as transparent stick models for comparison. (**B**) Structure-based sequence alignment of PH domains from β-spectrin (PDB code 1BTN), ARHGAP21 and DAPP1 (dual adaptator of phosphotyrosine and 3-phosphoinositides 1; PDB code 1FAO). β-spectrin and DAPP1 are respectively complexed to Ins(1,4,5)P3 (IP3) and Ins(1,3,4,5)P4 (IP4), and are the two first best scored provided by the DALI search with the PH domain of ARHGAP21 (*Z*-score of 14.8 and 14.1 for β-spectrin and DAPP1, respectively). The phosphoinositide-binding residues are highlighted in pink and yellow for β-spectrin and DAPP1, respectively. These residues are not conserved in ARHGAP21.

working together to determine protein–protein interactions; combination of two binding motifs may be required for target interaction. Such combination can present a much larger surface area to serve as a protein–protein interface and/or it may serve to confer greater specificity of binding as each motif contributes its own specificity to the interaction.

The five Arf:effector complex structures solved to date (Hanzal-Bayer *et al*, 2002; Panic *et al*, 2003; Shiba *et al*, 2003; Wu *et al*, 2004; O'Neal *et al*, 2005) reveal that effectors recognize a large hydrophobic surface of Arf proteins that encompasses the hydrophobic pocket composed of residues in the switch I, interswitch and switch II regions (Supplementary Figure S4 and Figure 2). Both biochemical and structural data have identified the hydrophobic pocket of Arf proteins as a structural determinant of effector binding with a key hydrophobic residue facing the hydrophobic pocket (this study; Kawasaki *et al*, 2005). Such an interaction confers specificity as revealed in the structure of the ARL1:Golgin245-GRIP domain complex, in which the key

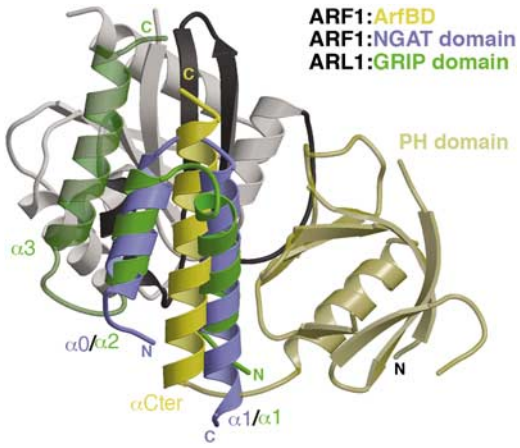

Figure 6 Modes of binding in various Arf:effector complexes. Superposition of the ARF1:ArfBD, the ARF1:GGA-NGAT domain and the ARL1:Golgin245-GRIP domain structures on their Arf binding partners. Note that for clarity, only ARF1 (shown in grey with its switch I–interswitch–switch II region in dark grey) from the ARF1:ArfBD complex is shown and the biological dimer unit of ARL1:GRIP domain structure is not shown. ArfBD is indicated in yellow with its αCter helix opaque and its PH domain transparent. The NGAT domain is shown in blue and the GRIP domain in green.

hydrophobic Tyr2177 residue of Golgin245 fits the hydrophobic pocket of ARL1 owing to a sequence variation compared to other Arf proteins (Panic *et al*, 2003). Another region for effector binding to Arf proteins is the adjacent hydrophobic triad patch composed of Phe51, Trp66 and Tyr81 (ARF1 numbering) of the interswitch and switch II regions (Figure 2). In the ARL1:Golgin245-GRIP domain complex, the interaction of the triad patch of ARL1 with Met2194 of Golgin245 is critical (Wu *et al*, 2004). Thus, the hydrophobic triad patch, similar to the hydrophobic pocket, appears as a structural determinant for effector binding. Strikingly, Rab proteins also possess a hydrophobic triad patch that is a major structural determinant for effector binding (Merithew *et al*, 2001). The sequence and position of the hydrophobic triad patches are conserved in Rab and Arf family GTPases, except for the position of the Phe residue that is two residues upstream in Rab proteins. The hydrophobic triad residues of the Rab proteins are conserved in sequence, but exhibit different side-chain rotamers that confer specificity to the effector recognition (Merithew *et al*, 2001). Such side-chain structural plasticity has not been observed in Arf proteins, but sequence variations are found in several members of the Arl and SAR subfamilies (Figure 2B), suggesting that the hydrophobic triad patch in Arf proteins is probably also a site of specificity. In addition, the hydrophobic surface of Arf proteins that encompasses the hydrophobic pocket and the hydrophobic triad patch is exposed only in the GTP-bound state. Indeed, GTP hydrolysis drives dramatic rearrangements of the switch regions that hinder this hydrophobic surface (Supplementary Figure S2). Altogether, this suggests that the hydrophobic pocket and the hydrophobic triad patch are structural determinants for effector binding and recognition. Note that these two structural determinants probably do not confer specificity of binding on Arf subfamily members as only one minor sequence difference is observed between ARF1 and ARF6 in the hydrophobic pocket (Figure 2B). This suggests that specific effectors of ARF1 or ARF6 should

interact with additional regions to distinguish between the two proteins.

ARHGAP21 interacts with both ARF1 and ARF6 as shown by our biochemical analysis and confirmed structurally (Dubois *et al*, 2005; this study). In HeLa cells, ARHGAP21 associates predominantly with the Golgi complex through some interaction with Golgi-associated ARF1. ARHGAP21 has been detected at cell–cell contacts between epithelial cells, and this localization required a physical interaction of ARHGAP21 with the junctional protein α-catenin (Sousa *et al*, 2005). As activated ARF6 is also known to localize at cell–cell junctions in epithelial cells, a role for ARF6 in this localization is possible and has not been tested (Palacios *et al*, 2001). Modelling the ARF1:ArfBD complex interaction with the membranes predicts that the C-terminal part of ArfBD should be directed towards the lipid bilayer. As a consequence, the C-terminal RhoGAP domain of ARHGAP21 when bound to ARF1 would be in close proximity to membrane-anchored Rho proteins. Thus, binding to ARF1 could facilitate ARHGAP21 interaction with Cdc42, and thus induce GTP hydrolysis to promote actin filament dynamics on Golgi membranes.

Materials and methods

Constructs and mutagenesis

The Arf-binding and RhoGAP domains (ArfBD/RhoGAP domains, residues 929–1346), the Arf-binding domain (ArfBD, residues 929–1096) and the PH domain alone (residues 929–1052) of human ARHGAP21 were subcloned from pEGFP vectors (Dubois *et al*, 2005) into the *Eco*RI–*Sal*I sites of pGST//1, a prokaryotic expression vector. The Y999A and I1053A variants of ArfBD were generated by substituting Tyr999 or Ile1053 with alanine using the QuickChange site-directed mutagenesis kit (Stratagene) from plasmid pEGFP-ArfBD (Dubois *et al*, 2005). For bacterial expression, ArfBD-Y999A and ArfBD-I1053A were subcloned from pEGFP constructs into the *Eco*RI–*Sal*I sites of pGST//1.

The N-terminally truncated and GTP-locked mouse ARF1 mutant, Δ17-ARF1-Q71L (called hereafter ARF1), gene clone was a kind gift of Dr Soichi Wakatsuki (Institute of Materials Structure Science, High Energy Accelerator Research Organization (KEK), Japan).

Subcellular localization

HeLa cells plated onto coverslips were transfected with pEGFP constructs using the calcium phosphate procedure. Cells were processed for immunofluorescence studies 16–20 h after transfection and stained with anti-GM130 medial Golgi marker (clone 35, BD Transduction Laboratories) followed by Cy3-conjugated anti-mouse IgG (Jackson ImmunoResearch Laboratories) as described (Dubois *et al*, 2005). Cells were examined under a motorized upright wide-field microscope (Leica DMRA2) with an oil-immersion objective (× 100 PL APO HCX, 1.4 NA) and a highly sensitive cooled interlined CCD camera (Roper CoolSnap HQ). Z-positioning was accomplished by mean of a piezo-electric motor (LVDT, Physik Instrument) mounted underneath the objective lens. The system was steered by Metamorph 5.0.7 Software (Universal Imaging Corporation, Downingtown, PA). Z-series of images (12–15 planes) were taken at 0.2 μm increments.

Expression and purification

For analytical ultracentrifugation experiments, GTPase assays and crystallization, ARHGAP21 domains were expressed as glutathione *S*-transferase (GST)-fusion protein in *E. coli* BL21 cells. Cells were harvested after induction with 0.5 mM IPTG for 5 h at 30°C. Frozen bacteria were resuspended in 50 mM Tris–HCl pH 8 containing 100 mM NaCl, 1 mM EDTA, 1 mM PMSF and 0.5 mg/ml lysozyme and were disrupted by sonication. The lysate was ultracentrifuged at 100 000 *g* for 30 min at 4°C and the supernatant was incubated at 4°C with glutathione Sepharose 4B beads for 2 h. The GST-fusion protein was eluted with gluthatione, cleaved with rTev protease overnight at 4°C and passed over a MonoQ 5/5 column (Amersham Biosciences). The flow-through containing ARHGAP21 domains was concentrated to 8 mg/ml, frozen in liquid nitrogen and stored at −80°C in 25 mM Tris–HCl pH 8, 100 mM NaCl, 5 mM $MgCl_2$ and 2 mM DTT.

Expression and purification of ARF1 have been described by Shiba *et al* (2003). Briefly, after purification by an Ni-NTA affinity column, the His6 tag was removed by rTev protease and ARF1 was further purified by gel filtration chromatography, concentrated to 8 mg/ml, frozen in liquid nitrogen and stored at −80°C in 25 mM Tris–HCl pH 8, 100 mM NaCl, 5 mM $MgCl_2$ and 2 mM DTT.

Analytical ultracentrifugation

Sedimentation equilibrium centrifugation of ARF1:ARHGAP21 complexes at a concentration of 1 mg/ml in 25 mM Tris–HCl pH 8, 100 mM NaCl, 5 mM $MgCl_2$ and 2 mM DTT was performed using a Beckman analytical ultracentrifuge model Optima XL-A, equipped with a 60 Ti four-hole rotor. Sedimentation equilibrium runs were carried out at 20 000 r.p.m. at 15°C, using cells with two-channel and 12-mm path-length centerpieces. Radial scans were taken at 280 nm at 3 h intervals. Equilibrium was reached after 24 h of centrifugation. The baseline offset was recorded at 60 000 r.p.m. at the end of the experiment. The solvent density was 1.01081 g/cm^3 and ARF1:ArfBD-wt (0.7311 cm^3/g), ARF1:ArfBD-Y999A (0.7342 cm^3/g), ARF1:ArfBD-I1053A (0.7333 cm^3/g) and ARF1:PH domain (0.7287 cm^3/g) complexes partial specific volume were calculated using the SEDNTERP software. The data were analysed with XLAEQ and EQASSOC programs (Beckman) to calculate weight-average molecular weights and association constants.

GTPase assays

E. coli BL21(DE3) strain was transformed with a pGEX plasmid encoding GST-fused Cdc42 and the protein was produced and purified by standard procedures. Purified GST-Cdc42 protein (1.5 μM) was loaded with 15 μM [γ-^{32}P]GTP in low-magnesium buffer (50 mM Hepes/NaOH pH 7.5, 100 mM KCl, 1 mM $MgCl_2$, 2 mM EDTA and 1 mM DTT) at 30°C for 2 min. $MgCl_2$ (1 mM free Mg^{2+}) was added to initiate GTP hydrolysis. For measurements of ArfBD/RhoGAP domains-stimulated GTP hydrolysis, 150 nM of ArfBD/RhoGAP domain in the presence or the absence of 1.5 μM of GTPγS-loaded Δ17-ARF1 was added 30 s after $MgCl_2$. At the indicated times, aliquots of 25 μl were removed and $^{32}P_i$ release was measured by the charcoal method (Higashijima *et al*, 1987).

Crystallization, data collection and processing

The ARF1:ArfBD complex was formed by incubation of ARF1 and ArfBD at a stoichiometric ratio of 2:1 overnight at 4°C. Proteins were loaded onto a Hiload 16/60 Superdex 75 prep-grade column (Amersham Biosciences) equilibrated with 50 mM Tris–HCl pH 7.5, 100 mM NaCl, 5 mM $MgCl_2$ and 2 mM DTT. The peak fractions containing the complex were concentrated to 20 mg/ml, flash-frozen and then stored at −80°C. Dynamic light-scattering experiments (DLS, DynaPro -801) indicated that the ARF1:ArfBD complex is monodisperse and has a hydrodynamic radius of 3.3 nm and an apparent molecular mass of 45 kDa, suggesting that the ARF1:ArfBD complex exits as a 1:1 complex in solution.

Crystallization conditions for the ARF1:ArfBD complex were found using a sparse matrix screen. Drops were prepared by mixing an equal volume of the complex solution (5–30 mg/ml) with the reservoir solution using the hanging drop vapor diffusion method at 16 and 4°C. Initial unique and big crystals of ARF1:ArfBD complex were obtained spontaneously within a few hours with a reservoir containing 15–20% PEG4000 (or 1.0 M Na citrate or 1.0 M NH_4 acetate), 10 mM $MgCl_2$, 2% dioxane and 100 mM of different buffers ranging from pH 4.6 to 9.5. Note that precipitant agent and buffer can vary to a large extent without affecting greatly the crystallization and crystal quality, but the presence of dioxane is essential. The quality of the initial crystals was poor with low resolution power and high mosaicity and twining. The best crystals however provided diffraction data to 3.0 Å, allowing structure determination (trigonal crystal form; data not shown). Information provided by the crystal packing and use of the reverse screen method (Stura *et al*, 1994; Ménétrey *et al*, 2007) allowed us to improve greatly the crystallization conditions and diffraction data. Improved

crystals were grown using 15% PEG5000 MME, 100 mM imidazole pH 6.8, 150 mM NH_4SO_4 or Li_2SO_4, 10 mM $MgCl_2$, 0.5% dioxane and 5% ethylene glycol. Cryoprotection was performed using crystallization conditions complemented with 20% ethylene glycol in a two-step process. First, the cryoprotectant solution was added at the tips of the crystallization drop and the crystals were pushed gradually through the cryoprotectant solution gradient, then the crystals were transferred to a drop containing only the cryoprotectant solution and they were flash-frozen in liquid nitrogen. Diffraction data were collected at −170°C for initial and improved crystals on ID14-2 and ID29 beamlines of the European Synchrotron Radiation Facility (ESRF). Intensities were integrated with MOSFLM and scaled with SCALA (CCP4, 1994). The improved crystals, which diffract up to 2.1 Å, belong to the primitive monoclinic space group $P2_1$ with six complexes in the asymmetric unit and $a = 74.64$ Å, $b = 132.14$ Å, $c = 146.28$ Å and $\beta = 90.01°$ cell parameters.

Structure determination and refinement

In the trigonal crystal form, molecular replacement for ARF1 was performed and solved with PHASER with the automated search process (McCoy *et al*, 2005) using as search model Δ17-$ARF1_{GTP}$-Q71L (Shiba *et al*, 2003; PDB code 1J2I). No solution was obtained for the ArfBD domain using as search model several PH domain structures with PHASER or any other molecular replacement programs. However, it was possible to position manually a PH domain model (Hyvonen *et al*, 1995; PDB code 1BTN) in the continuous-difference electron density calculated using phases from the ARF1 molecular replacement solution. The F_o-F_c map indicated two long and discontinuous regions of extra electron density that we anticipated to be the position for helices. As the PH domain encompasses only one helix, we positioned this helix in the two extra electron density regions in both orientations and conserved the position that matched best with smaller isolated extra electron density regions and acceptable crystal packing contacts. We then improved this position using rigid body refinement with CNS (Brünger *et al*, 1998). Improved electron density maps and decrease of the *R* factors confirmed that we had found the solution. Then, the C-terminal part of the ArfBD was built manually as a long helix in the second extra electron density region that was linked to the C-terminus of the PH domain providing *de facto* the orientation of this last helix. The structure was refined by maximum likelihood refinement with CNS (Brünger *et al*, 1998) and Refmac (CCP4, 1994) and by graphical building using TURBO (Roussel and Cambillaud, 1989). Then, the monoclinic crystal form was obtained and molecular replacement was performed with PHASER using as a model the ARF1:ArfBD structure built in the trigonal crystal form. The complex was further refined to 2.1 Å. ARP-wARP was used for automatic building of water molecules (Perrakis *et al*, 1999).

The refined structure consists of six ARF1:ArfBD complexes with 1669 residues, six Mg.GTP, six sulphates, three dioxanes and 1656 water molecules. Some side chains are poorly defined in the current structure and were modelled with null occupancy making no contact with vicinal residues. Note that in ARF1, two N-terminal residues (Gly, Ser) resulting from the TEV cleavage site of the His tag were modelled in electron density and numbered as residues 16 and 17. The two first residues 929–930 and regions 944–955, 979–986 and 1064–1096 from ArfBD have no defined electron density and were omitted from the model. The stereochemistry of the final refined model is excellent and there are no Φ–Ψ pairs outside the allowed regions of the Ramachandran plot. The refined structure has a crystallographic *R*-value of 20.0% and a free *R*-value of 23.5%. Crystallographic statistics are summarized in Table I. Figures were produced using Molscript (Kraulis, 1991) and Raster3D (Merritt and Bacon, 1997).

Supplementary data

Supplementary data are available at *The EMBO Journal* Online (http://www.embojournal.org).

Acknowledgements

We thank Aurélie Rayer, Karine Regazzoni and Satoko Murakami for their expert technical help, Wolfgang Faigle for mass spectrometry measurements and Lucien Cabanié and Ahmed El Marjou for help with protein purification. We are also grateful to the Institut de Biologie Physico-Chimique (IBPC, Paris, France) and Ines Gallay for providing access to the X-ray generator, the Laboratoire d'Enzymologie et Biochimie Structurale (LEBS, Gif-sur-Yvette, France) for providing access to their analytical ultracentrifugation equipment and to the staff of ID14, ID23 and ID29 beamlines at the European Synchrotron Radiation Facility (ESRF) for providing synchrotron beam time and help during the collection of data. We thank Dr Soichi Wakatsuki for the kind gift of the ARF1 gene clone, Dr Enrico Stura for help in crystallization and Dr Jacqueline Cherfils for discussions and critical comments on the manuscript. This work was supported by the Association pour la Recherche contre le Cancer to AH (grant 3564) and a grant from La Ligue Nationale contre le Cancer ('équipe labellisée') to PC.

Co-ordinates: The coordinates and structure factors have been deposited in the Protein Data Bank (accession numbers 2J59 and r2j59sf, respectively).

Notes: This structure was the target for CAPRI (Critical Assessment of PRediction of Interactions, http://capri.ebi.ac.uk/; Round 9 T24 and T25 predictions).

References

Antonny B, Beraud-Dufour S, Chardin P, Chabre M (1997) N-terminal hydrophobic residues of the G-protein ADP-ribosylation factor-1 insert into membrane phospholipids upon GDP to GTP exchange. *Biochemistry* **36:** 4675–4684

Brünger AT, Adams PD, Clore GM, DeLano WL, Gros P, Grosse-Kunstleve RW, Jiang JS, Kuszewski J, Nilges M, Pannu NS, Read RJ, Rice LM, Simonson T, Warren GL (1998) Crystallography and NMR system: a new software suite for macromolecular structure determination. *Acta Crystallogr D* **54:** 905–921

CCP4 (1994) The CCP4 suite: program for protein crystallography. *Acta Cristallogr D* **50:** 760–763

D'Souza-Schorey C, Chavrier P (2006) ARF proteins: roles in membrane traffic and beyond. *Nat Rev Mol Cell Biol* **7:** 347–358

Dubois T, Paleotti O, Mironov AA, Fraisier V, Stradal TE, De Matteis MA, Franco M, Chavrier P (2005) Golgi-localized GAP for Cdc42 functions downstream of ARF1 to control Arp2/3 complex and F-actin dynamics. *Nat Cell Biol* **7:** 353–364

Godi A, Di Campli A, Konstantakopoulos A, Di Tullio G, Alessi DR, Kular GS, Daniele T, Marra P, Lucocq JM, De Matteis MA (2004) FAPPs control Golgi-to-cell-surface membrane traffic by binding to ARF and PtdIns(4)P. *Nat Cell Biol* **6:** 393–404

Goldberg J (1998) Structural basis for activation of ARF GTPase: mechanisms of guanine nucleotide exchange and GTP-myristoyl switching. *Cell* **95:** 237–248

Hall A (2005) Rho GTPases and the control of cell behaviour. *Biochem Soc Trans* **33:** 891–895

Hanzal-Bayer M, Renault L, Roversi P, Wittinghofer A, Hillig RC (2002) The complex of Arl2-GTP and PDE delta: from structure to function. *EMBO J* **21:** 2095–2106

Higashijima T, Ferguson KM, Smigel MD, Gilman AG (1987) The effect of GTP and Mg^{2+} on the GTPase activity and the fluorescent properties of Go. *J Biol Chem* **262:** 757–761

Hyvonen M, Macias MJ, Nilges M, Oschkinat H, Saraste M, Wilmanns M (1995) Structure of the binding site for inositol phosphates in a PH domain. *EMBO J* **14:** 4676–4685

Kahn RA, Cherfils J, Elias M, Lovering RC, Munro S, Schurmann A (2006) Nomenclature for the human Arf family of GTP-binding proteins: ARF, ARL, and SAR proteins. *J Cell Biol* **172:** 645–650

Kawasaki M, Nakayama K, Wakatsuki S (2005) Membrane recruitment of effector proteins by Arf and Rab GTPases. *Curr Opin Struct Biol* **15:** 681–689

Kraulis PJ (1991) MOLSCRIPT: a program to produce both detailed and schematic plots of protein structures. *J Appl Crystallogr* **24:** 946–950

Lemmon MA (2004) Pleckstrin homology domains: not just for phosphoinositides. *Biochem Soc Trans* **32:** 707–711

Levine TP, Munro S (2002) Targeting of Golgi-specific pleckstrin homology domains involves both PtdIns 4-kinase-dependent and -independent components. *Curr Biol* **12:** 695–704

Li H, Tochio N, Koshiba S, Inoue M, Kigawa T, Yokoyama S, (RSGI), R.S.G.P.I. Solution structure of the PH domain of Rho GTPase activating protein 21 from human to be published

McCoy AJ, Grosse-Kunstleve RW, Storoni LC, Read RJ (2005) Likelihood-enhanced fast translation functions. *Acta Crystallogr D* **61:** 458–464

Ménétrey J, Perderiset M, Cicolari J, Houdusse A, Stura EA (2007) Improving diffraction from 3 to 2 Å for a complex between a small GTPase and its effector by analysis of crystal contacts and use of reverse screening. *Protein Sci*, in press

Merithew E, Hatherly S, Dumas JJ, Lawe DC, Heller-Harrison R, Lambright DG (2001) Structural plasticity of an invariant hydrophobic triad in the switch regions of Rab GTPases is a determinant of effector recognition. *J Biol Chem* **276:** 13982–13988

Merritt EA, Bacon DJ (1997) Raster3D: photorealistic molecular graphics. *Methods Enzymol* **277:** 505–524

O'Neal CJ, Jobling MG, Holmes RK, Hol WG (2005) Structural basis for the activation of cholera toxin by human ARF6-GTP. *Science* **309:** 1093–1096

Ostermeier C, Brunger AT (1999) Structural basis of Rab effector specificity: crystal structure of the small G protein Rab3A complexed with the effector domain of rabphilin-3A. *Cell* **96:** 363–374

Palacios F, Price L, Schweitzer J, Collard JG, D'Souza-Schorey C (2001) An essential role for ARF6-regulated membrane traffic in adherens junction turnover and epithelial cell migration. *EMBO J* **20:** 4973–4986

Panic B, Perisic O, Veprintsev DB, Williams RL, Munro S (2003) Structural basis for Arl1-dependent targeting of homodimeric GRIP domains to the Golgi apparatus. *Mol Cell* **12:** 863–874

Pasqualato S, Renault L, Cherfils J (2002) Arf, Arl, Arp and Sar proteins: a family of GTP-binding proteins with a structural device for 'front-back' communication. *EMBO Rep* **3:** 1035–1041

Perrakis A, Morris RM, Lamzin VS (1999) ARP/wARP can be employed for automatic density interpretation and tracing of a protein model. Resolution around 2.0 Å is the current limit… but we are working on it! *Nat Struct Biol* **6:** 458–463

Roussel A, Cambillaud C (1989) Turbo. In *Silicon Graphics Geometry Partner Directory*, pp 77–78. Mountain View, CA Silicon Graphics

Shiba T, Kawasaki M, Takatsu H, Nogi T, Matsugaki N, Igarashi N, Suzuki M, Kato R, Nakayama K, Wakatsuki S (2003) Molecular mechanism of membrane recruitment of GGA by ARF in lysosomal protein transport. *Nat Struct Biol* **10:** 386–393

Sousa S, Cabanes D, Archambaud C, Colland F, Lemichez E, Popoff M, Boisson-Dupuis S, Gouin E, Lecuit M, Legrain P, Cossart P (2005) ARHGAP10 is necessary for alpha-catenin recruitment at adherens junctions and for Listeria invasion. *Nat Cell Biol* **7:** 954–960

Stamnes M (2002) Regulating the actin cytoskeleton during vesicular transport. *Curr Opin Cell Biol* **14:** 428–433

Stura EA, Satterthwait AC, Calvo JC, Kaslow DC, Wilson IA (1994) Reverse screening. *Acta Crystallogr D* **50:** 448–455

Takai Y, Sasaki T, Matozaki T (2001) Small GTP-binding proteins. *Physiol Rev* **81:** 153–208

Vetter IR, Nowak C, Nishimoto T, Kuhlmann J, Wittinghofer A (1999) Structure of a Ran-binding domain complexed with Ran bound to a GTP analogue: implications for nuclear transport. *Nature* **398:** 39–46

Vetter IR, Wittinghofer A (2001) The guanine nucleotide-binding switch in three dimensions. *Science* **294:** 1299–1304

Villa Braslavsky CI, Nowak C, Gorlich D, Wittinghofer A, Kuhlmann J (2000) Different structural and kinetic requirements for the interaction of Ran with the Ran-binding domains from RanBP2 and importin-beta. *Biochemistry* **39:** 11629–11639

Wu M, Lu L, Hong W, Song H (2004) Structural basis for recruitment of GRIP domain golgin-245 by small GTPase Arl1. *Nat Struct Mol Biol* **11:** 86–94